

Article

Experimental Research into an Innovative Green Propellant Based on Paraffin–Stearic Acid and Coal for Hybrid Rocket Engines

Grigore Cican ^{1,2,*}, Alexandru Paraschiv ¹, Adrian Nicolae Buturache ³, Andrei Iaroslav Hapenciu ⁴, Alexandru Mitrache ² and Tiberius-Florian Frigioescu ¹

¹ Romanian Research and Development Institute for Gas Turbines COMOTI, 220D Iuliu Maniu Avenue, 061126 Bucharest, Romania; alexandru.paraschiv@comoti.ro (A.P.); tiberius.frigioescu@comoti.ro (T.-F.F.)

² Faculty of Aerospace Engineering, National University of Science and Technology Politehnica Bucharest, 1-7 Polizu Street, 1, 011061 Bucharest, Romania

³ FasterEdu, 075100 Otopeni, Romania; office@fasteredu.com

⁴ Vanguard Technology Association, 82205 Gilching, Germany; andrei.hapenciu@vanguard.technology.org

* Correspondence: grigore.cican@comoti.ro or grigore.cican@upb.ro

Abstract: This study focuses on an innovative green propellant based on paraffin, stearic acid, and coal, used in hybrid rocket engines. Additionally, lab-scale firing tests were conducted using a hybrid rocket motor with gaseous oxygen as the oxidizer, utilizing paraffin-based fuels containing stearic acid and coal. The mechanical performance results revealed that the addition of stearic acid and coal improved the mechanical properties of paraffin-based fuel, including tensile, compression, and flexural strength, under both ambient and sub-zero temperatures ($-21\text{ }^{\circ}\text{C}$). Macrostructural and microstructural examinations, conducted through optical and scanning electron microscopy (SEM), highlighted its resilience, despite minimal imperfections such as impurities and micro-voids. These characteristics could be attributed to factors such as raw material composition and the manufacturing process. Following the mechanical tests, the second stage involved conducting a firing test on a hybrid rocket motor using the new propellant and gaseous oxygen. A numerical simulation was carried out using ProPEP software to identify the optimal oxidant-to-fuel ratio for the maximum specific impulse. Following simulations, it was observed that the specific impulse for the paraffin and for the new propellant differs very little at each oxidant-to-fuel (O/F) ratio. It is noticeable that the maximum specific impulse is achieved for both propellants around the O/F value of 2.2. It was observed that no hazardous substances were present, unlike in traditional solid propellants based on ammonium perchlorate or aluminum. Consequently, there are no traces of chlorine, ammonia, or aluminum-based compounds after combustion. The resulting components for the simulated motor include H_2 , H_2O , O_2 , CO_2 , CO , and other combinations in insignificant percentages. It is worth noting that the CO concentration decreases with an increase in the O/F ratio for both propellants, and the differences between concentrations are negligible. Additionally, the CO_2 concentration peaks at an O/F ratio of around 4.7. The test proceeded under normal conditions, without compromising the integrity of the test stand and the motor. These findings position the developed propellant as a promising candidate for applications in low-temperature hybrid rocket technology and pave the way for future advancements.

Keywords: paraffin; hybrid rocket engine; propellant; green; stearic acid; coal



Citation: Cican, G.; Paraschiv, A.; Buturache, A.N.; Hapenciu, A.I.; Mitrache, A.; Frigioescu, T.-F. Experimental Research into an Innovative Green Propellant Based on Paraffin–Stearic Acid and Coal for Hybrid Rocket Engines. *Inventions* **2024**, *9*, 26. <https://doi.org/10.3390/inventions9020026>

Academic Editors:

Andrzej Łukaszewicz, Mohamed Thariq Hameed Sultan, Quang Ha, Wojciech Giernacki, Leszek Ambroziak, Wojciech Tarasiuk and Andriy Holovatyy

Received: 30 December 2023

Revised: 20 February 2024

Accepted: 21 February 2024

Published: 29 February 2024



Copyright: © 2024 by the authors. Licensee MDPI, Basel, Switzerland. This article is an open access article distributed under the terms and conditions of the Creative Commons Attribution (CC BY) license (<https://creativecommons.org/licenses/by/4.0/>).

1. Introduction

Hybrid rocket motors, incorporating both solid fuel grains and liquid or gaseous oxidizers, have gained significant attention for their promising applications in the field of propulsion [1–6]. The fuel is housed within the combustion chamber in the form of a cylinder, featuring one or more hollowed-out channels, known as ports, along its axis. The

oxidizer is introduced into the combustion chamber through a single-fluid feed system. The pioneering development of a hybrid rocket engine is credited to Sergei Korolev, whose rocket, named GRID09, first took flight in 1933 [5]. Generating 500 N of thrust and reaching an altitude of 1500 m, the rocket utilized liquid oxygen as the oxidizer, a compound still in use today. The solid-state fuel comprised a mixture of crude oil and rosin (colophony). Current space launchers use solid propellant in one or several of their stages and almost all of them use an ammonium perchlorate (AP, NH_4ClO_4)-based propellant, often combined with aluminum (Al) powder, leading to the emission of various chlorinated hazardous exhaust products [7–9]. Efforts are being made to replace these polluting propellants with alternatives that offer similar properties but are environmentally friendly [10,11]. The flagship of the European Space Agency, Ariane-5, and the recently commissioned Vega launcher utilize considerable amounts of composite propellant (476 and 122 tons, respectively), resulting in the release of 270 and 71 tons of concentrated hydrochloric acid per launch. Even the American Space Shuttle's solid rocket boosters contained 998 tons of ammonium perchlorate-based propellant, leading to the discharge of 580 tons of concentrated hydrochloric acid upon complete combustion [12]. Several studies have investigated diverse fuels used in hybrid rocket engines, including HTPB. Many studies refer to different fuels used in hybrid rocket engines, including HTPB (hydroxyl-terminated polybutadiene)/paraffin [13], mixtures with varying concentrations of crystalline wax and paraffin wax, PolyEthylene wax, High-Density PolyEthylene, Poly-Methyl MethAcrylate (PMMA) fuel grains, and sorbitol [14,15]. To enhance the performance of hybrid rocket engines, various additives are developed, as their performance is generally lower compared to liquid fuel engines. Energetic additives, including aluminum at micro and nano scales, have demonstrated the ability to increase the regression rate of hybrid fuels while serving as a dense energy source [5,14]. Additionally, boron is considered for improved regression owing to its higher volumetric heat release in comparison to aluminum, despite its limited usability due to ignition difficulties [16]. Metal hydrides [17,18], such as magnesium hydride (MgH_2) and lithium aluminum hydride (LiAlH_4), are being explored for performance enhancement, resulting in an augmented regression rate of paraffin wax. Moreover, the use of polymers [19] increases the melt viscosity of the wax, thereby reducing the effect of droplet entrainment, and thus the regression rate. Paraffin stands out as a promising fuel under investigation for use in hybrid propellant rockets owing to its advantageous attributes such as high regression rate, throttling capabilities, non-toxicity, manufacturability, and cost-effectiveness.

A recent study [20] suggests potential applications of paraffin-based hybrid rocket propulsion across various market segments, including upper stages, sub-orbital launch vehicles, tactical missiles, small satellite injection systems, and boosters, with anticipated cost reductions future shortly. Furthermore, the use of hybrid propulsion for interplanetary missions is currently being evaluated [14]. Numerous experimental investigations into paraffin-based hybrid rocket motors have been undertaken, including regression-rate measurements, analyses of fuel properties, and an increased focus on visualizing the combustion process [21–24]. However, a published review [15] reported the limited availability of data on the structural performance of hybrid fuel grains, because this has not been a primary concern in the development of hybrid propulsion. In other studies [25,26], the need to investigate the structural performance of paraffin-based propellants was justified by the possible fragmentation of the initially cracked grain, which may result in either fuel loss or nozzle blocking, with the subsequent over-pressurization of the combustion chamber. Operating under low temperatures, hybrid propellant rockets launched from high altitudes (balloon launch, air launch) or employed in the upper stages of launch vehicles (space tugs, orbital transfer vehicles) may encounter challenges that compromise the structural integrity of the propellant grain, leading to the formation of cracks which may also originate during the manufacturing process. While certain additives can be utilized to improve the mechanical properties, this improvement may come to the detriment of other important parameters of the propellant, including the regression rate. Furthermore, as highlighted

by Andrianov et al. [27], specific conditions during the manufacturing process can lead to the formation of radial cracks in relatively small solid propellant grains, resulting in local overheating of the structural casing and potentially jeopardizing the structural integrity of the motor. Additionally, the presence of a radial crack in a paraffin grain can induce alterations in the initial shape of the grain's port due to the combustion within the crack. Therefore, the issue of crack formation in the solid propellant grain of a hybrid propulsion system should not be ignored. However, the utilization of paraffin as a fuel on a large scale is hindered by its high brittleness and low mechanical strength [28]. To address its suboptimal structural performance, some additives can be used to improve the mechanical properties of the propellant, even if to the detriment of other important parameters of the propellant, such as the regression rate [29]. Several studies have investigated the development of various paraffin-based fuels. For instance, Y. Pa et al. [28] studied the thermal, mechanical, and ballistic performance of paraffin–aluminum (P–Al), paraffin–boron (P–B), and paraffin–carbon black (P–CB) fuels. They found that the addition of polymer and metallic additives improved the mechanical strength of the fuels, accelerated oxidation, and enhanced the heat release rate during combustion.

This study aims to assess the mechanical properties and microstructural characteristics of pure paraffin specimens and specimens comprising a mixture of pure paraffin, stearic acid, and coal, both before and after exposure to negative temperature treatment. Additionally, a lab-scale hybrid rocket motor using gas oxygen as an oxidizer has been used to conduct firing tests with paraffin-based fuels containing stearic acid and coal components. The new propellant is designed to be one that does not produce pollutants such as chlorine, hydrochloric acid, ammonia, aluminum, etc., as byproducts of the combustion reaction.

2. Materials and Methods

2.1. Fuel Preparation

For the development of a new propellant, an examination of pure paraffin as a reference and a combination of pure paraffin, stearic acid, and coal was conducted, focusing on mechanical properties, microstructural characteristics, and ignition performance. The addition of stearic acid and coal powder to the mixture, as detailed in Table 1, was intended to improve the structural and thermal stability of the paraffin-based fuels, and the specific properties of these compounds are shown in Table 2.

Table 1. Paraffin fuel formulations tested.

| Sample | Paraffin (%) | Stearic Acid (%) | Coal Powder (%) |
|----------------|--------------|------------------|-----------------|
| Reference | 100 | 0 | 0 |
| New propellant | 88 | 10 | 2 |

Table 2. Properties of the fuel matrix and additives according to the literature.

| Properties | Paraffin | Stearic Acid | Charcoal–Coal Powder |
|------------------------------|---------------------------------|--|--|
| Chemical formula | C ₂₀ H ₄₂ | C ₁₈ H ₃₆ O ₂ | C ₇₁ H ₃ O ₁₃ N |
| Density (g/cm ³) | 0.9172 [30] 0.92 | 0.9408 [30] | 0.88 [31] |
| Melting point (°C) | 58.3 [30] | 69.0 [30] | - |
| Molecular weight (g/mol) | 282 | 284 | 1077 [31] |
| Combustion heat/(MJ/kg) | 47.36 [30] 59–66 | 40.6 [30] | 28 [31] |

The mixture was prepared through heating in an electric furnace at 350 K and continuously stirring for 15–20 min to achieve homogeneity. Subsequently, it was poured slowly and continuously into a casting mold. To prevent adhesion between the paraffin and the mold, a thin layer of diesel was applied to the inner edges of the casting mold,

simplifying the removal of the fuel grain after the paraffin solidified. A previous study [32] reported that paraffin wax exhibits volumetric shrinkage (15–25%) during the transition from a liquid to a solid phase, which varies based on the wax grade. Therefore, to avoid the formation of air bubbles and other discontinuities in the fuel grain during casting, the molten paraffin mixture was poured slowly and continuously into the casting mold in a single pour. Examination of the fractured surface of the fuel grain revealed no significant cracks or bubbles along the grain length.

2.2. Mechanical Performance Tests

Both the pure paraffin specimens and the paraffin specimens containing stearic acid and coal were subjected to tests for tensile, compressive, and flexural strength under two distinct conditions: storage at room temperature and exposure to sub-zero temperatures (−21 °C) for 24 h. For each type of material, test, and condition, three specimens, whose codifications are presented in Table 3, were evaluated.

Table 3. Codification of pure paraffin and paraffin mixture specimens with stearic acid and coal.

| Specimen Type | As Prepared (Kept at Room Temperature) | | | Cold Treated (Kept at −21 °C for 24 h) | | |
|-----------------------------------|--|------|------|--|------|------|
| Reference (pure paraffin) | Pa_1 | Pa_2 | Pa_3 | Pc_1 | Pc_2 | Pc_3 |
| New propellant (paraffin mixture) | Ma_1 | Ma_2 | Ma_3 | Mc_1 | Mc_2 | Mc_3 |

To assess the mechanical properties of the new propellant, three types of specimens were designed for tensile, compression, and bending tests. The dimensions and geometry of these specimens are detailed in Figure 1.

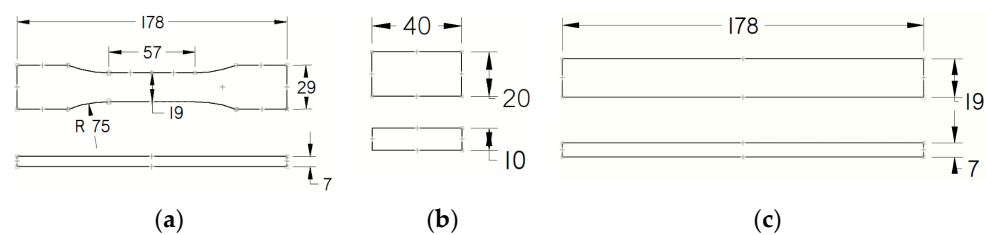


Figure 1. The dimensions and geometry of the specimens utilized for the mechanical test: (a) tensile specimens, (b) compression specimens, and (c) three-point bending specimens.

The specimens were produced using the additively manufactured ABS (acrylonitrile butadiene styrene) molds presented in Figure 2.

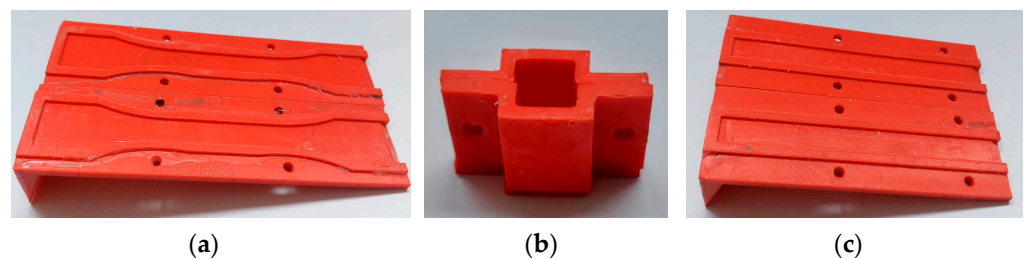


Figure 2. Additively manufactured molds for manufacturing specimens for mechanical tests: (a) molds for tensile specimens, (b) molds for compression specimens, and (c) molds for bending specimens.

After preparing the molds, both paraffin and the new propellant were introduced into the molds and heated to 350 K using an electric kettle. Continuous mixing was maintained throughout the melting process until both the paraffin and the new propellant reached a liquid state. The crucial step in this process was to ensure continuous mixing, particularly

for the new propellant, to achieve a more homogeneous mixture. Subsequently, the molten material was poured into the molds, stirred thoroughly, and allowed to slowly cool to room temperature. Figure 3 illustrates the raw paraffin wax used and shows images capturing various stages in the preparation of the paraffin and new propellant.



Figure 3. Preparation of paraffin and paraffin mixture: (a) paraffin wax solid grain, (b) prepared paraffin wax, and (c) heating at 76.8°C and mixing the paraffin and new propellant.

Before casting, the molds were coated with diesel to prevent the propellant from adhering. For each testing type, eight specimens of both pure paraffin and the new propellant were prepared. Half of these samples were tested at room temperature, while the others were subjected to testing at -21 degrees Celsius. Figure 4 illustrates the specimens obtained for testing.



Figure 4. The paraffin and new propellant specimens used for the mechanical tests.

All mechanical tests were performed using an Instron 3369 mechanical testing system (Instron, Norwood, MA, USA), which was equipped with dedicated devices for tensile, bending, and compression testing, as depicted in Figure 5.

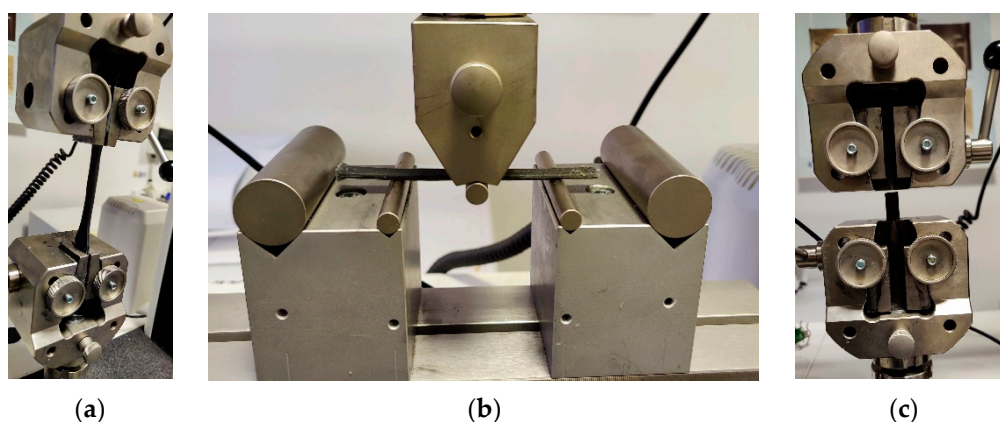


Figure 5. Mechanical testing of specimens: (a) tensile testing, (b) three-point bending testing, and (c) compression testing.

2.3. Mechanical Performance Tests

The pure paraffin specimens and the paraffin mixture were investigated in an as-prepared state and after testing using scanning electron microscopy (SEM) with an FEI Inspect F50 scanning electron microscope—SEM (FEI Company, Brno, Czech Republic), and optical microscopy using a Motic SMZ-171 7.5X-50X Zoom Stereo Microscope (Motic Asia Kowloon, Hong Kong, China). Due to the nature of the fracture of tensile specimens, particular attention was focused on the analysis of the fracture surfaces. Therefore, sections from the damaged specimens were cut and affixed onto a double-sided conductive carbon tape to hold the sample on the stub and were scanned using an acceleration voltage of 20 kV. Because paraffin wax is a nonconductive material, the surface morphology of the specimens was analyzed via SEM after the samples were sputter-coated with gold using the SC7620 Mini Sputter Coater/Glow Discharge System (Quorum Technologies, Laughton, East Sussex, UK).

2.4. Numerical Simulation Performance

To study the performance of a rocket engine, a set of numerical simulations was conducted in the initial phase. The simulations were performed using the ProPEP software, aiming to comparatively observe, both for pure paraffin and for the new recipe, the maximum specific impulse (Isp), the maximum combustion temperature in the combustion chamber, and the concentration of CO and CO₂ in the combustion products from the combustion chamber as a function of the variation of the oxidizer/fuel (O/F) ratio from 0 to 8. This was conducted for a rocket engine with a combustion chamber pressure of 10 bar and an exhaust pressure of 1 bar.

2.5. Engine Test

For the new mixture, sticks of the new propellant were created and assessed using a lab-scale ballistic test motor to verify the stability and functionality of the new propellant during operation on the test bench.

In this regard, a stick of the new propellant was cast, as shown in the figure below. A mold obtained from a 3D printer was used for casting. To obtain the central hole of the stick, a metal rod was used, as illustrated in Figure 6a. The dimensions of the stick were 2.54 cm for the outer diameter and 1 cm for the inner diameter. In addition, a cylindrical shape with a coaxial central port was additively manufactured for casting the new propellant.

Figure 6 presents the mold obtained from 3D printing and the stick of the new propellant.

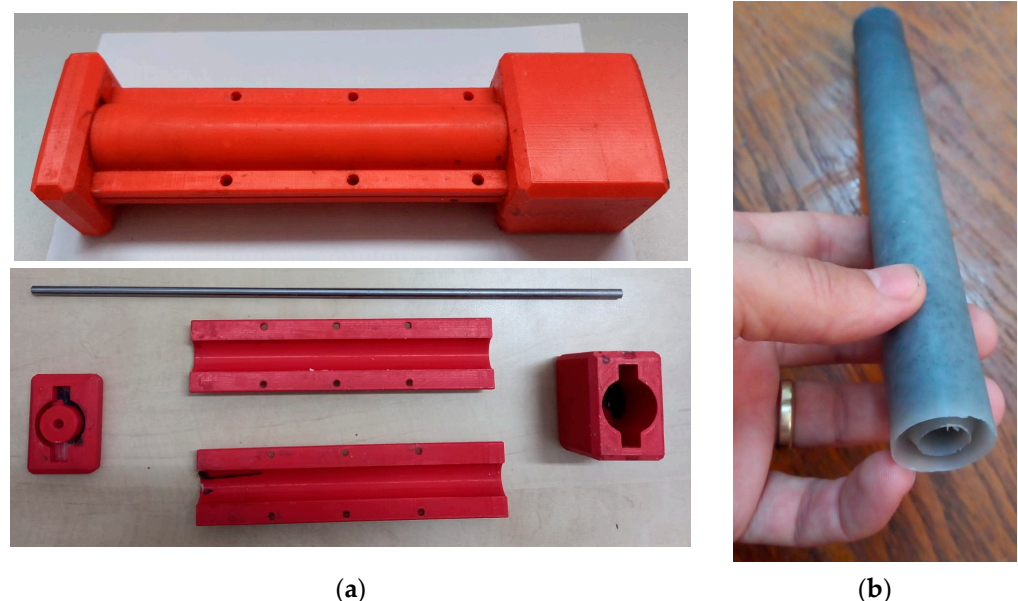


Figure 6. (a) Mold and (b) stick for the new propellant.

In Figure 7, the testing stand for the rocket engine is depicted. More details about the testing stand can be found in the sources [33,34].

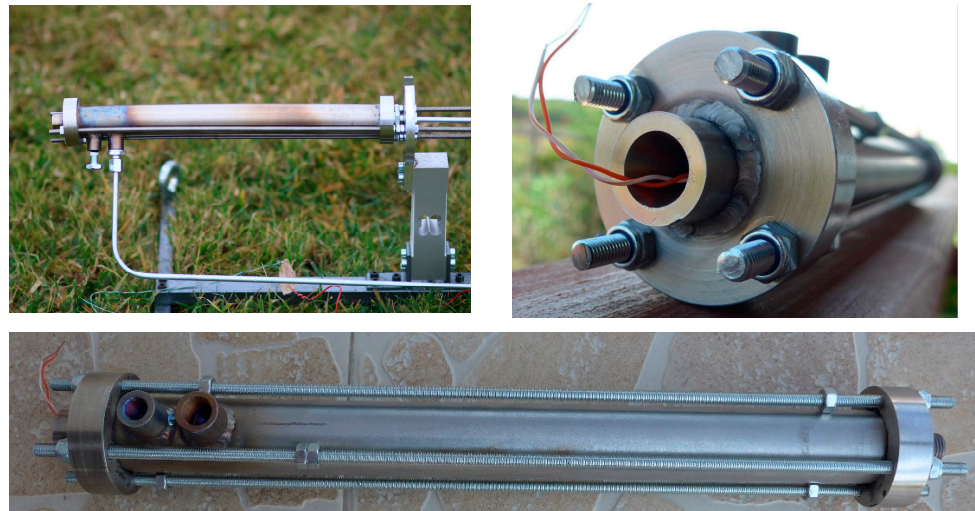


Figure 7. The test bench.

Gaseous oxygen was utilized as the oxidizer. The experimental hybrid motor arrangement at the laboratory scale consisted of an oxidizer supply system, a stainless steel combustion chamber, a convergent–divergent nozzle, and an ignition system, as illustrated in Figure 8.

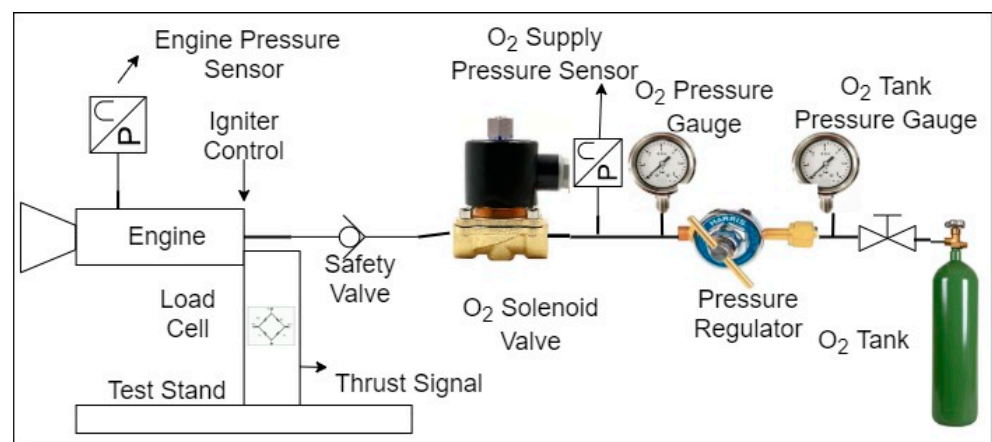


Figure 8. Test bench block diagram.

The oxidizer mass flow rate entering the combustion chamber was systematically regulated through the utilization of a pressure regulator. Gaseous oxygen was introduced into an oxidizer-settling chamber with a diameter of 55 mm and a length of 33 mm. Injection into the combustion chamber was facilitated with an axial-flow injector plate. The cylindrical combustion chamber, with an inner diameter of 42 mm and a length of 150 mm, housed the solid fuel. To maintain an 8 mm gap between the fuel port and the nozzle entry, the fuel grain length was consistently upheld at 142 mm within the combustion chamber. This post-combustion chamber facilitated the interaction of unburnt paraffin with liquid oxygen before exiting the nozzle.

A meticulous firing test procedure was adhered to, to ensure the accuracy of the test. The firing device employed a mixture of potassium nitrate and sugar, a standard formulation widely used in igniting solid rocket engines for rocketry challenges. The selected proportions for the mixture were 60% potassium nitrate and 40% sugar to enhance

safety, as the igniter's performance was not a focal point of this study. While various additives like corn syrup, aluminum powder, and nitrocellulose could augment the igniting mixture to influence burning time or heat generation, the decision was made to adhere to the proportions recommended by Richard Nakka to streamline the process.

The ignition process involved nickeline wires powered by a 12 V source, as illustrated in Figure 9. The application of current through the nickeline wire rendered it incandescent, initiating the ignition of the mixture. It is imperative to maintain a constant heating source temperature during the preparation of an ignition mixture from potassium nitrate and sugar, following established manufacturing guidelines. Deviations from these temperature indications or the use of an open flame instead of an electric stove are potential causes of accidents associated with this process.



Figure 9. Fuel rod ignition system: (a) potassium nitrate and sugar; (b) nickeline wires for ignition.

The test bench features a horizontal metallic frame equipped with a vertical load cell. The motor is positioned horizontally, exerting force perpendicular to the load cell. This design minimizes the test bench's footprint and allows for the jet plume to be directed away from the pressurized oxygen tank. The load cell has a maximum measuring force of 250 kgf, chosen to accommodate various sizes of rocket engines without compromising accuracy. With a sensitivity of 2 m V/V, the load cell produces a maximum signal of 10 mV at 250 kg for a 5 V excitation voltage. Assuming a 6-sigma accuracy of the data acquisition system at 0.4 μ V, the measurement accuracy is estimated at 10 g with a resolution of approximately 1 g, employing a sampling period of 9.227 ms. While faster sampling speeds are attainable, they come at the expense of reduced accuracy.

3. Results

3.1. Mechanical Performance

3.1.1. Tensile Testing

Histograms depicting average tensile test results for both the pure paraffin and paraffin mixture specimens in their as-prepared and cold-treated states are presented in Figure 10a–d. The examination of load and ultimate tensile strength (UTS) revealed significant variations dependent on the chemical composition and testing temperature. Specifically, the M_c specimens, tested at negative temperature, exhibited the highest load (45.6 N) and UTS (2.1 MPa). In line with this trend, the P_c samples displayed substantial strength, but 50% lower than M_c. Conversely, the as-prepared specimens, both of pure paraffin (P_a) and the paraffin mixture (M_a), exhibited significantly lower values. Young Modulus analysis revealed a distinct hierarchy among the specimens, with M_c samples showing the highest modulus (165.9 MPa), reflecting greater stiffness, followed closely by P_c (147.7 MPa), M_a (63.1 MPa), and P_a (26.78 MPa).

The samples with the highest strength also exhibited the smallest elongations. The assessment of elongation at the point of tensile strength showcased a pattern evidenced by stress–elongation curves (Figure 11). The observed variations in elongation provide insights into the materials' deformation characteristics and may be crucial for understanding their mechanical behavior. Sample P_a exhibited the highest elongation, indicating greater ductility, followed

by P_c, M_a, and M_c. These findings suggest that P_a exhibits a more pliable behavior under tensile stress, while M_c displays a more rigid response at the cost of less resistance.

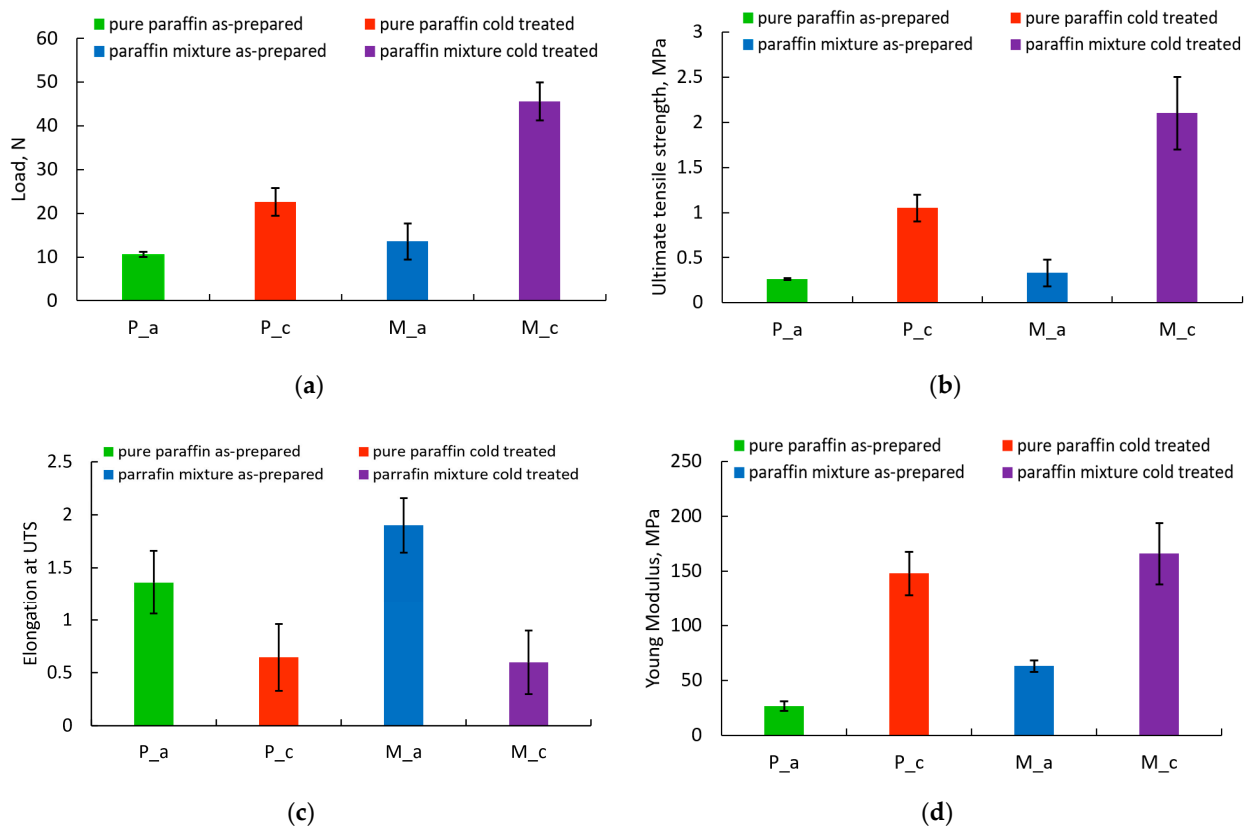


Figure 10. Tensile test results of pure paraffin and paraffin mixture specimens: (a) load, (b) ultimate tensile strength (c) elongation and (d) elastic modulus.

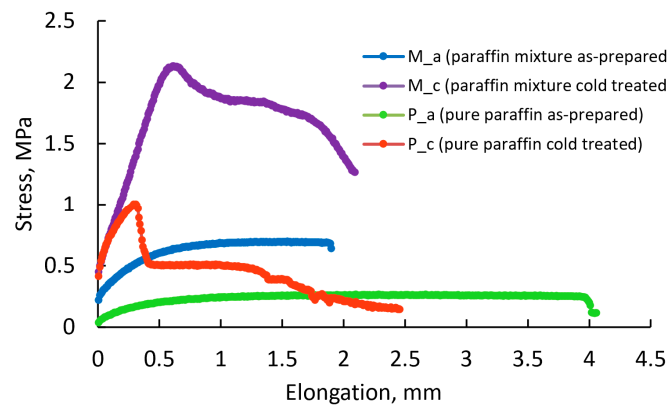


Figure 11. Stress–elongation curves for pure paraffin and paraffin mixture specimens.

The observed differences in mechanical behavior based on testing temperature necessitate further investigation into this influential parameter concerning other mechanical properties and microscopic characteristics.

3.1.2. Compression Testing

Figure 12 presents average compression test results for pure paraffin and paraffin mixture specimens in their as-prepared and cold-treated states, focusing on compression behavior and the influence of testing temperature. Similar to the trend observed in the tensile tests, M_c specimens exhibited the highest compression load at 246.7 N, indicating

superior strength. P_c specimens followed closely with a load of 157.0 MPa, demonstrating notable strength compared to the specimens tested at room temperature, but with considerably higher strength compared to M_a and P_a. Examining compression elongation, M_a demonstrated the highest value at 1.025 mm, reflecting greater deformation under compression. P_c, M_c, and P_a followed with values of 0.9 mm, 0.7 mm, and 0.5 mm, respectively. This suggests that M_c exhibits a more ductile response under compression, while P_a shows a more rigid behavior with less deformation. Intriguingly, the results related to the compressive elongations present an opposing trend to the findings obtained for tensile elongations.

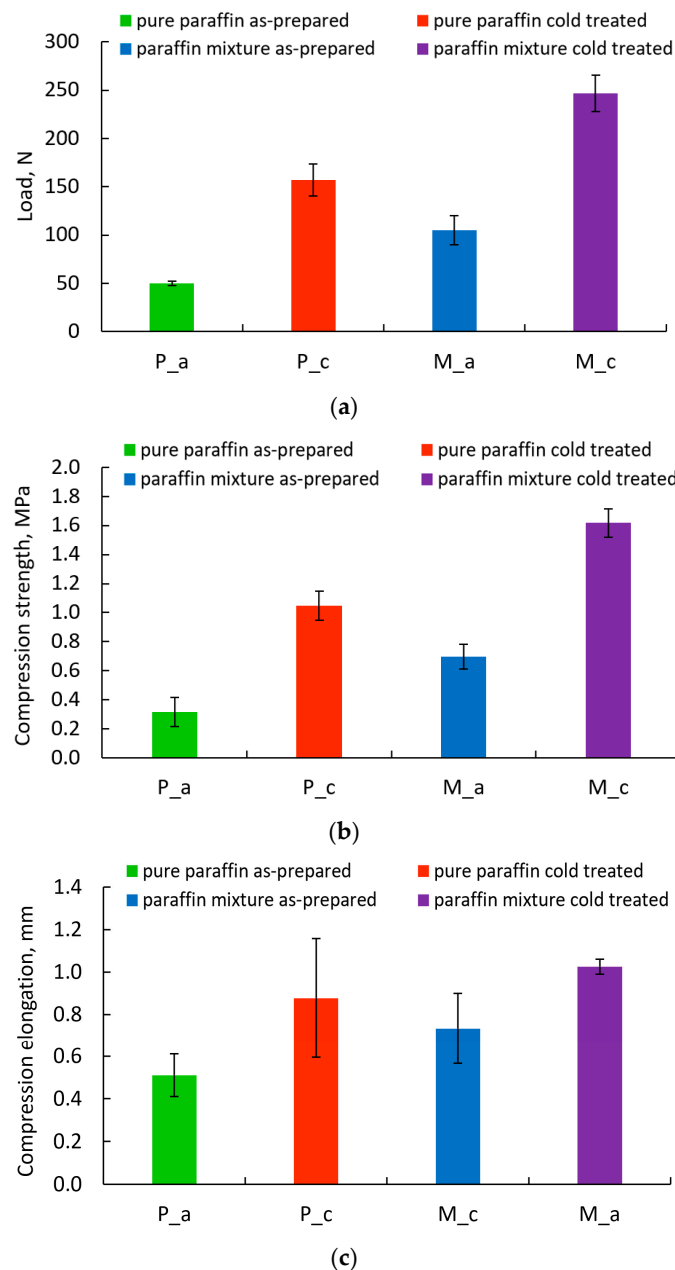


Figure 12. Compression test results of pure paraffin and paraffin mixture specimens: (a) load, (b) compression strength and (c) compression elongation.

During the compression test, the cold-treated specimens exhibiting the highest compressive strength values also demonstrated the highest compressive elongations, indicating

the complex interplay between material composition, testing temperature, and mechanical properties during different modes of deformation.

3.1.3. Three-Point Bend Testing

The three-point bending results of pure paraffin and the new propellant specimens highlight variations in elongation, respectively, suggesting a strong tendency to decrease ductility (Figure 13).

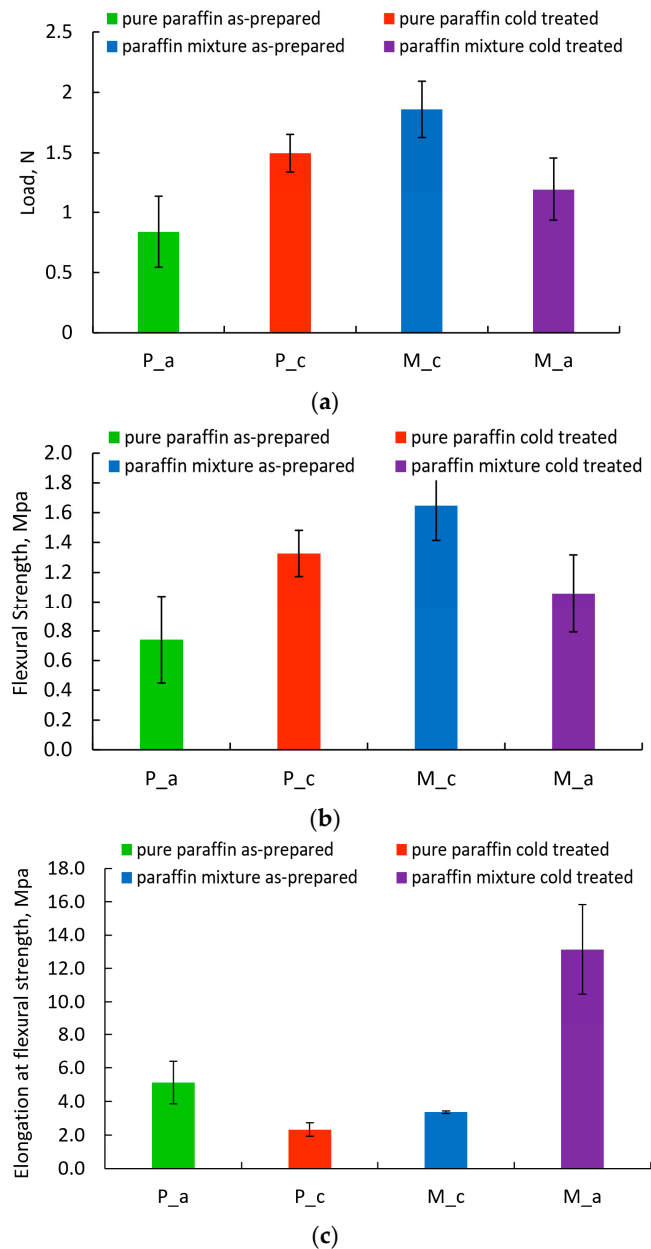


Figure 13. Three-point bend test results of pure paraffin and paraffin mixture specimens: (a) load, (b) flexural strength, and (c) elongation at flexural strength.

The mechanical tests, encompassing tensile, compression, and bending properties, revealed that the specimens of the new propellant developed in these experiments exhibited the highest strength when tested at a negative temperature. This consistent trend across the three mechanical testing types emphasizes the superior mechanical performance of the paraffin mixture in comparison to pure paraffin, both under ambient and cold-temperature conditions. These findings suggest that the developed propellant, specifically designed

for low-temperature applications, exhibits superior strength characteristics across various modes of mechanical loading, thereby substantiating its promising potential for practical use in hybrid rocket engines.

3.2. Macrostructural Investigation

The macrostructural investigation involved an examination and fractographical evaluation of both pure paraffin and the new propellant specimens in their as-prepared state and after undergoing cold testing. Optical images at $\times 10$ magnifications were captured to inspect the surface of the tensile specimens and the cross-sectional surface rupture after tensile testing at both room temperature and negative temperatures. Figures 14 and 15 showcase these images, revealing a predominantly homogeneous structure along the edges and a central region devoid of visible pellets or micro-cracks. Certain regions of the specimens, especially within the paraffin mixture, exhibited impurities and internal micro-voids, as can be seen in both surface (Figure 14a–d) and tensile fracture surfaces (Figure 15a–d) of the test specimens. However, as shown by the mechanical tests, these features did not significantly influence the mechanical strength of the paraffin mixture, which was superior in both ambient and negative temperatures.

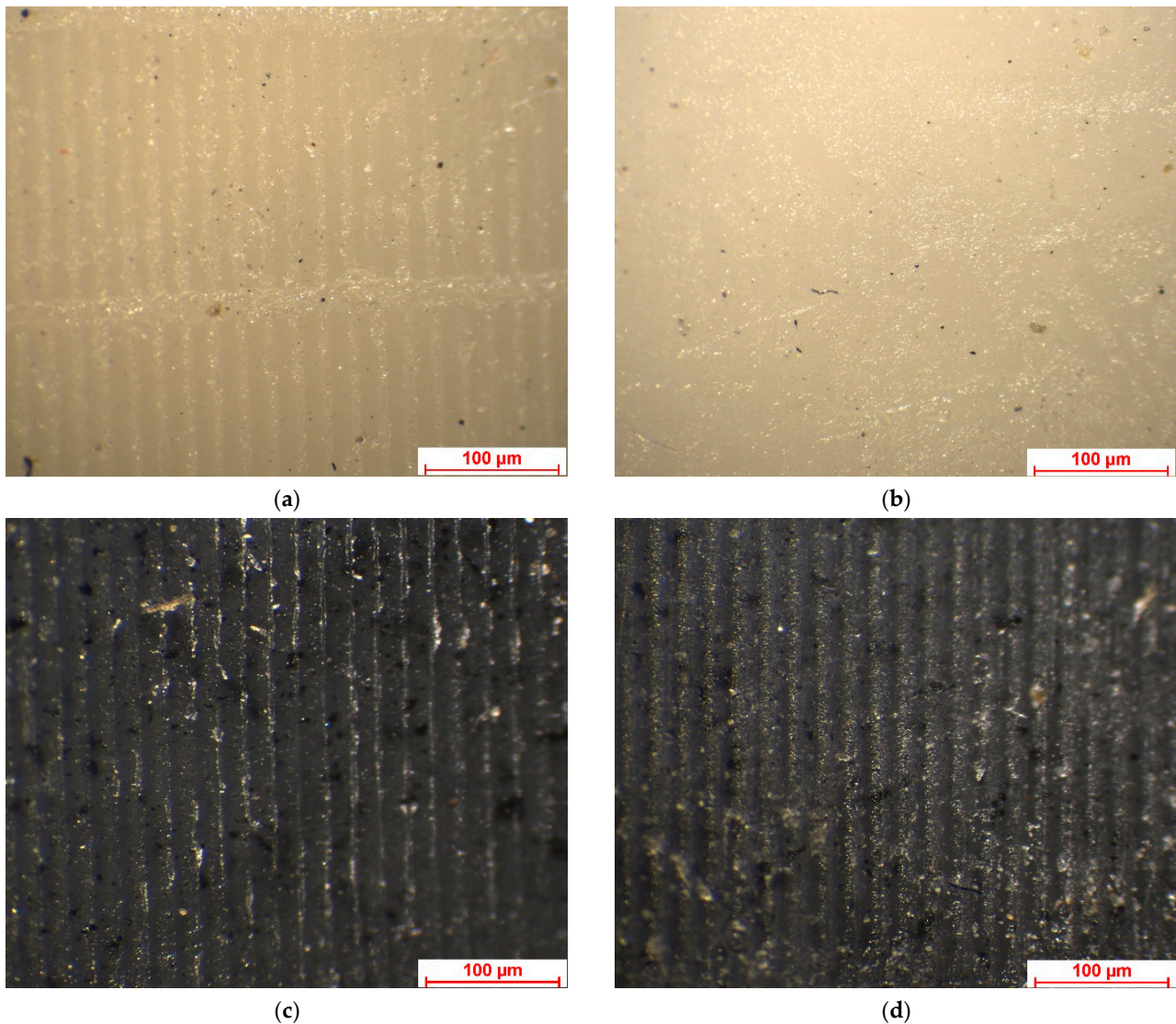


Figure 14. Representative optical images of surfaces of tensile specimens: (a) pure paraffin specimens in the as-prepared state, (b) pure paraffin specimens in the cold-treated state, (c) paraffin mixture specimens in the as-prepared state, and (d) paraffin mixture specimens in the cold-treated state.

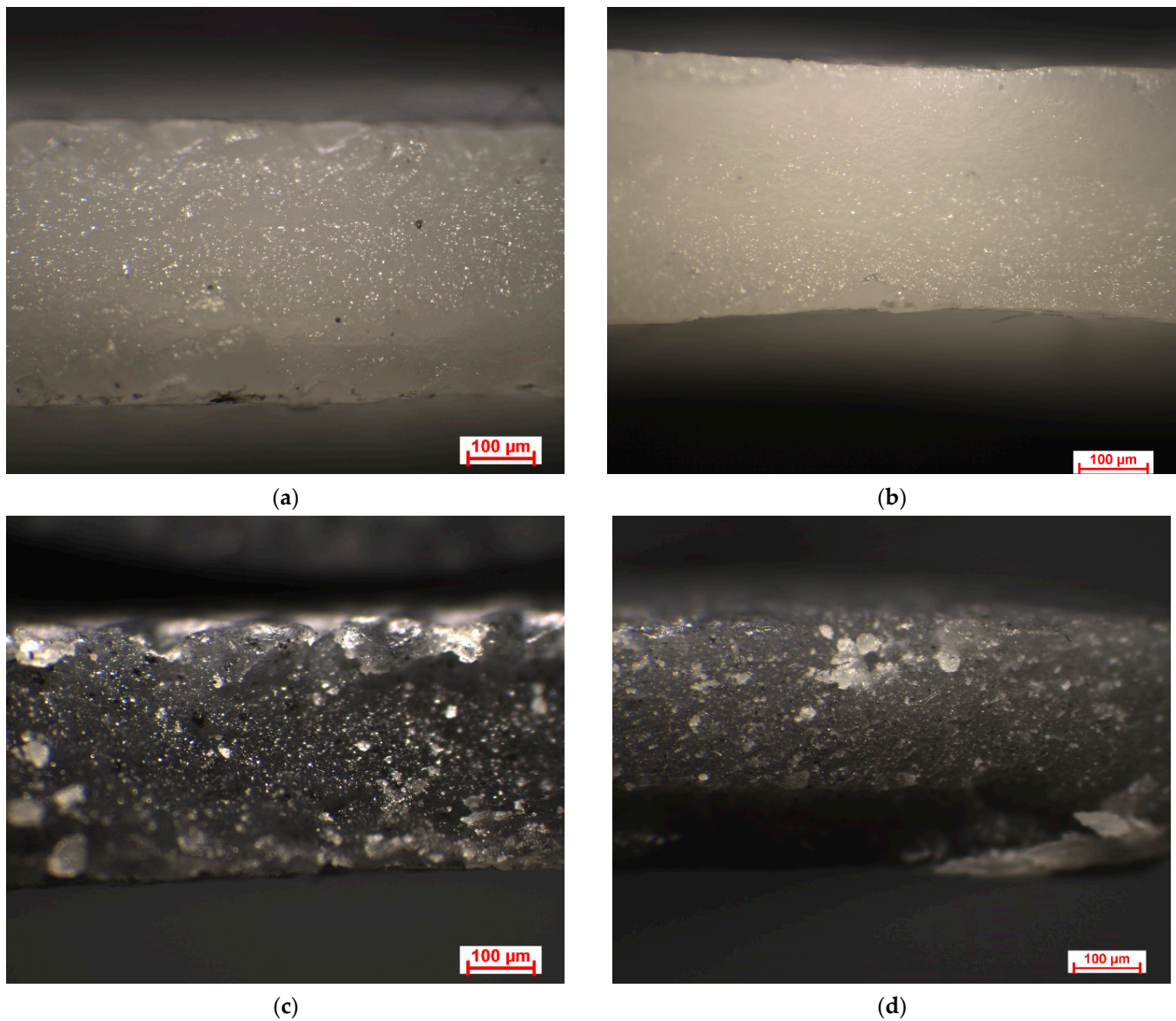


Figure 15. Representative optical images of fracture surfaces of tensile specimens: (a) pure paraffin specimens in the as-prepared state, (b) pure paraffin specimens in the cold-treated state, (c) paraffin mixture specimens in the as-prepared state, and (d) paraffin mixture specimens in the cold-treated state.

The observed impurities and micro-voids could be attributed to factors such as the raw material variations, the manufacturing process, or the specific composition of the paraffin mixture. Interestingly, despite their presence, the mechanical tests demonstrated that these imperfections did not compromise the material's strength, highlighting its resilience and potential for application in hybrid rocket systems, where structural integrity is crucial for reliable performance. Further investigation into the origin and distribution of these features using scanning electron microscopy could provide valuable insights into the material's structural characteristics.

Microstructural Investigation

Scanning electron microscopy (SEM) analysis was used to investigate the microstructure of fracture surfaces in both pure paraffin and the new propellant tensile specimens. The microstructural features are depicted in Figure 16 for pure paraffin specimens in both the as-prepared and cold-treated states, while Figure 17 displays SEM images of

fracture surfaces for new propellant specimens in both conditions. The SEM images in Figures 16 and 17 reveal a similar microstructure and morphology between pure paraffin and the new propellant. However, a noticeable increase in densification and a reduction in voids were observed in the fracture surfaces of both pure paraffin and the new propellant after cold treatment. Interestingly, specimens tested at room temperature exhibited a more fragile appearance compared to those tested at negative temperatures.

Despite the superior mechanical properties of pure paraffin specimens over paraffin mixture specimens, the microstructural investigation did not unveil any characteristics that could justify this behavior. Most probably, the mixture of pure paraffin with stearic acid and coal improved strong interfacial interaction between structural elements that increased the mechanical strength of the new fuel.

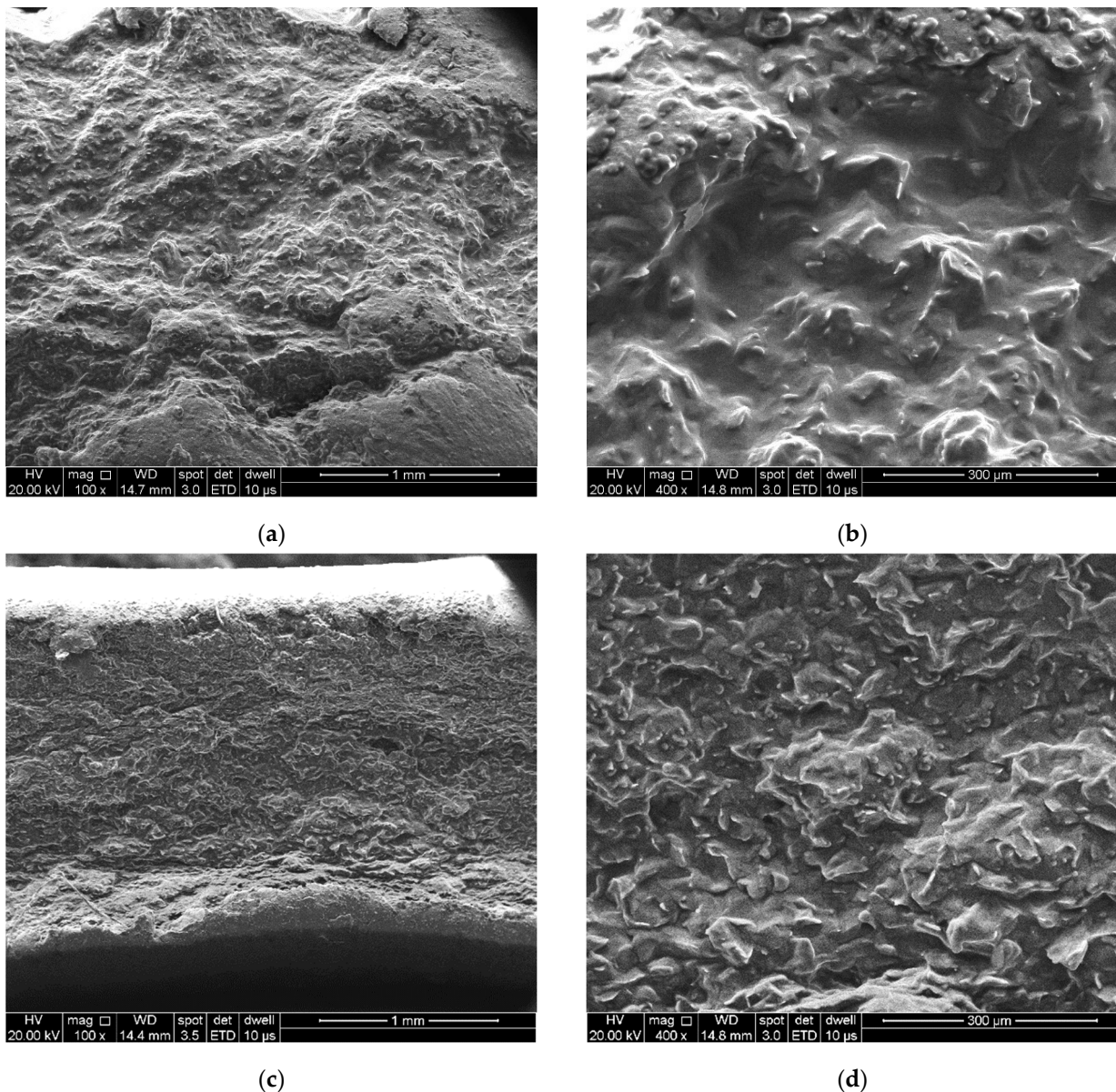


Figure 16. Representative SEM images of fracture surfaces of tensile specimens: (a,b) pure paraffin specimens in an as-prepared state, and (c,d) pure paraffin specimens in a cold-treated state.

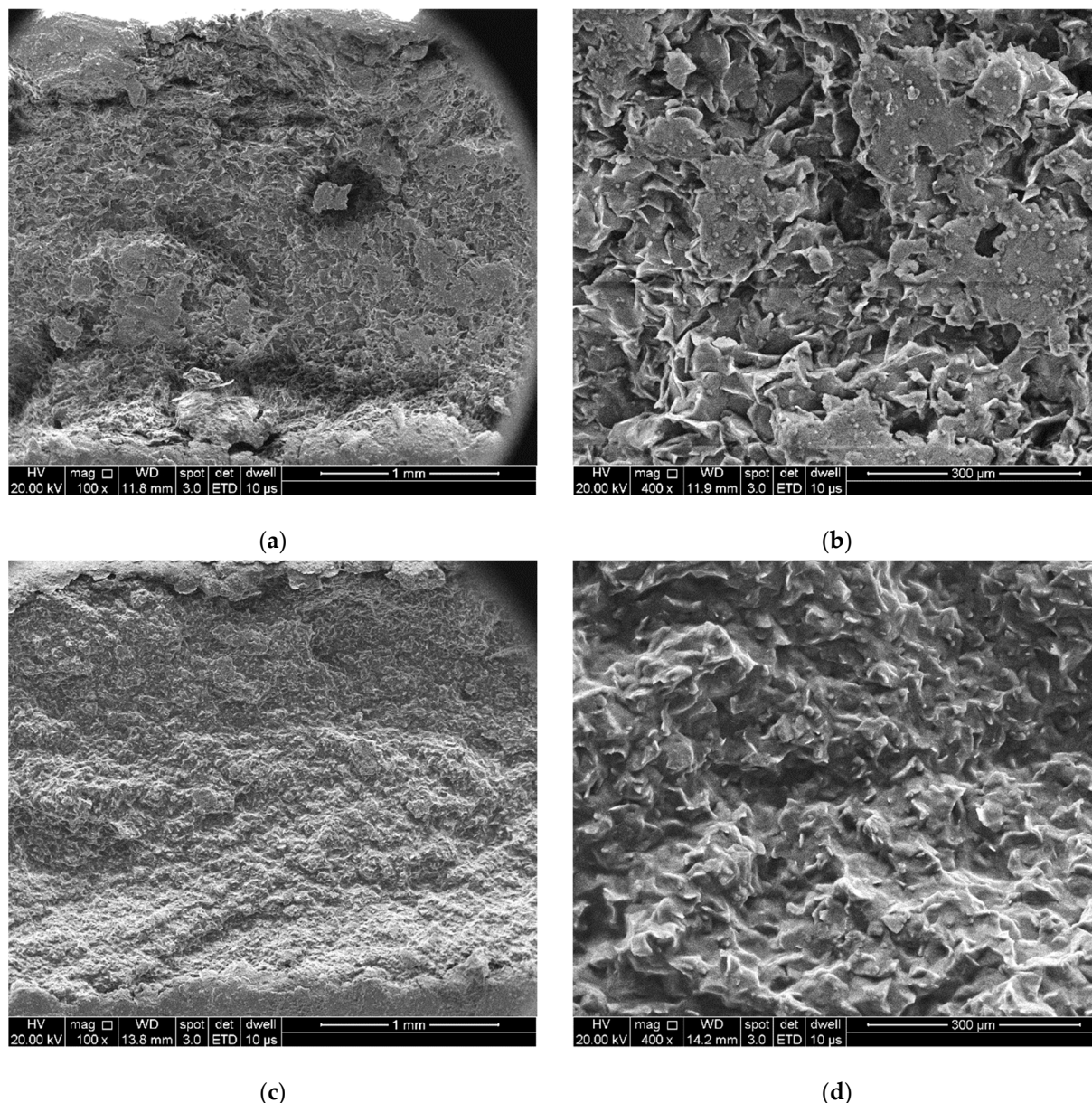


Figure 17. Representative SEM images of fracture surfaces of tensile specimens: (a,b) paraffin mixture specimen in as-prepared state, and (c,d) paraffin mixture specimen in cold-treated state.

3.3. Numerical Simulation Engine Performance

Following the numerical simulations in the ProPEP software, the obtained results are depicted in the following figures. Figures 18–21 illustrate the variation of specific impulse, combustion temperature, and the concentration of CO and CO₂ as a function of the O/F ratio.

It can be observed from the above figure that the specific impulse for the two propellants differs very little at each O/F ratio. It is noticeable that the maximum specific impulse is achieved for both propellants around the O/F value of 2.2. This ratio was considered for the experimental part as well.

It can be observed from the Figure 19 that the combustion temperatures between the two propellants do not differ significantly based on O/F. The maximum combustion temperature, T_{comb}, is around the O/F value of 2.8. Although the combustion temperature significantly contributes to the specific impulse value, the experimental O/F ratio chosen is not 2.8 but the previously mentioned value for ISP, namely, O/F = 2.2.

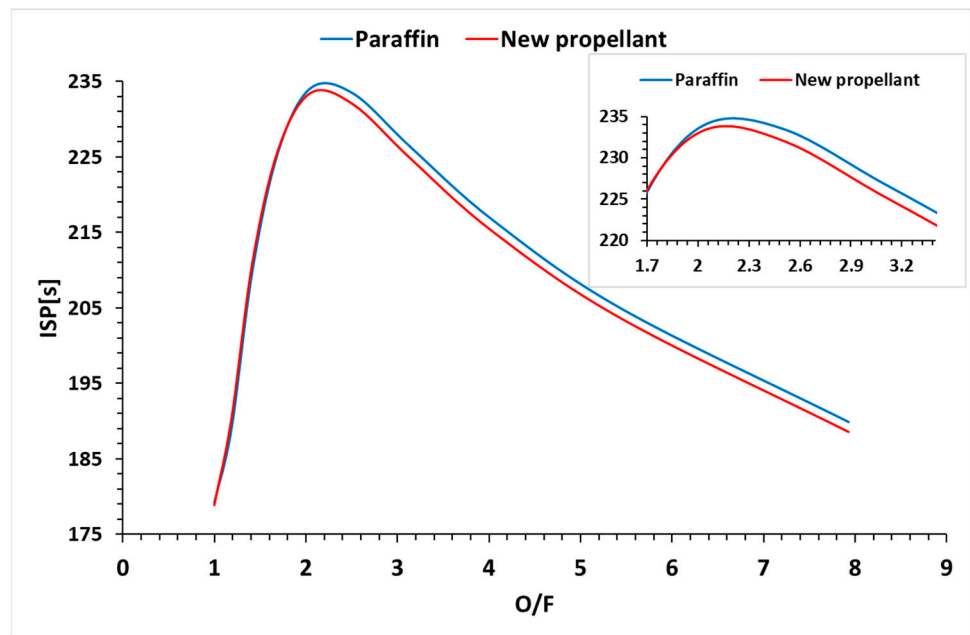


Figure 18. Specific impulse variation as a function of O/F ratio.

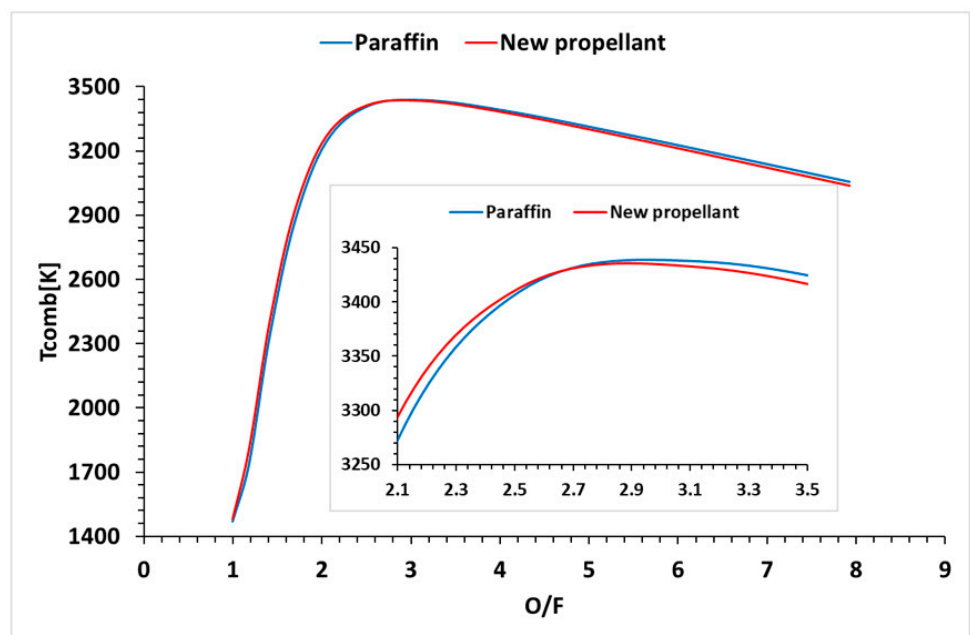


Figure 19. Combustion temperature variation in the combustion chamber (T_{comb}) as a function of O/F ratio.

Following the simulations of the combustion of paraffin and the new propellant, it was observed that there were no hazardous substances, as would be the case for traditional solid propellants based on ammonium perchlorate or aluminum. Thus, no chlorine, ammonia, or aluminum-based compounds appear after combustion. Consequently, for the simulated motor, the resulting components include H_2 , H_2O , O_2 , CO_2 , CO , and other combinations in insignificant percentages.

It can be noted that the CO concentration decreases with the increase in the O/F ratio for both propellants, and the differences between concentrations are not significant.

To better visualize the percentage differences for the variables of interest from Figures 12–21, the variation of the percentage difference was presented as a function of the O/F ratio. This ratio was selected at several points.

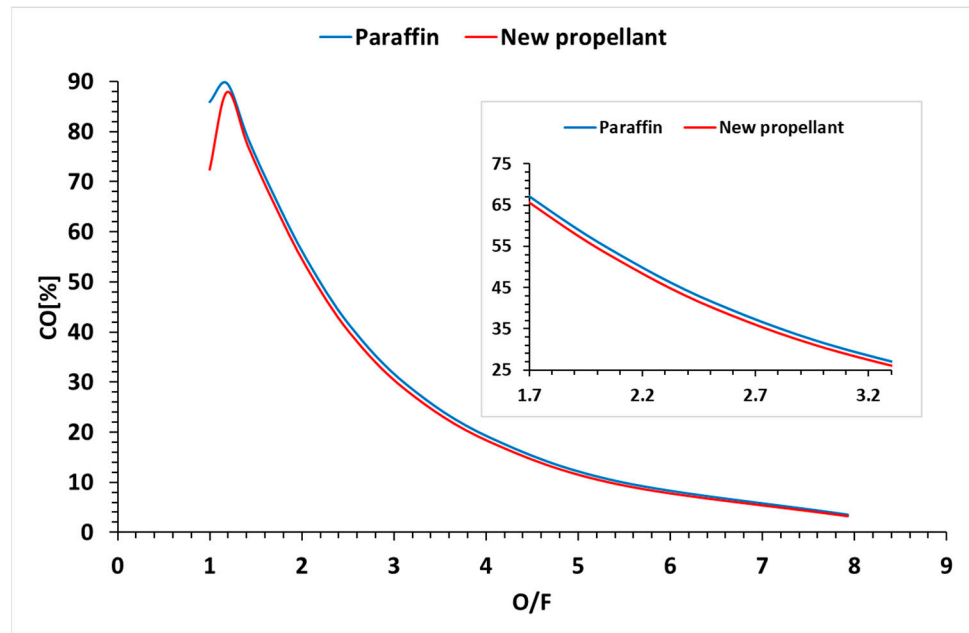


Figure 20. Variation of the mass concentration of CO in percentages as a function of the O/F ratio.

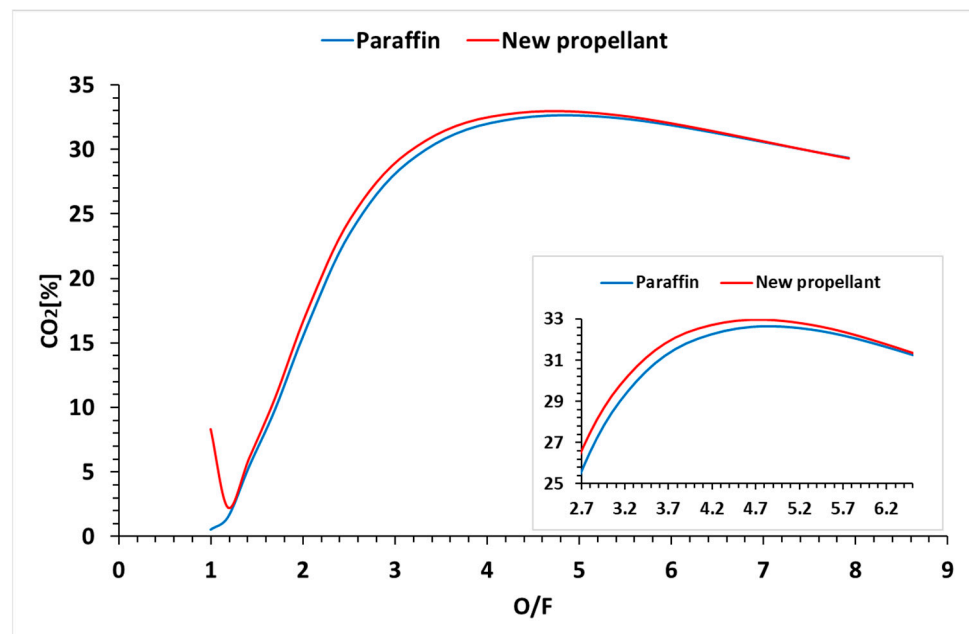


Figure 21. Variation of the mass concentration of CO₂ in percentages as a function of the O/F ratio.

Table 4 presents the percentage difference of paraffin compared to the new propellant for ISP, Tcomb, and for the mass concentration of CO and CO₂.

Table 4. The percentage difference of paraffin compared to the new propellant for ISP, Tcomb, and for the mass concentration of CO and CO².

| | % | | | | | | | | | |
|--------------------------|----------|--------|--------|-------|-------|-------|-------|-------|-------|------|
| ISP _{space} [s] | 0.17 | −0.74 | −0.52 | −0.13 | 0.26 | 0.60 | 0.66 | 0.69 | 0.63 | 0.68 |
| T _{comb} [K] | −0.68 | −4.00 | −2.87 | −1.78 | −0.77 | −0.12 | 0.15 | 0.30 | 0.43 | 0.62 |
| CO [%] | 15.64 | 1.85 | 1.91 | 2.30 | 2.90 | 3.50 | 3.87 | 4.44 | 5.42 | 7.75 |
| CO ² [%] | −1469.42 | −49.31 | −12.01 | −9.22 | −7.20 | −4.62 | −2.70 | −1.53 | −0.67 | 0.11 |
| O/f | 1.00 | 1.19 | 1.42 | 1.70 | 2.05 | 2.52 | 3.14 | 4.05 | 5.45 | 7.93 |

As can be observed for ISP, which is the most important variable, the errors are very small, below 1%.

As for the CO² concentration, it reaches a maximum for an O/F ratio around 4.7. For experimentation, as mentioned above, the O/F ratio of 2.2 was chosen, indicating a mass concentration value of around 15% of the total combustion gas mass.

3.4. Engine Test Performance

Due to the difficulty in precisely calculating the performance of the hybrid rocket engine, mainly because the burn rate of the new propellant needs to be known, conducting a ballistic test, which falls outside the scope of this study, is necessary. Consequently, the motor with the new propellant was tested to assess its stability during operation, to observe if the combustion was stable, and to identify any potential serious issues that could jeopardize the integrity of the motor.

Figure 22 depicts an image captured during the ignition of the rocket motor with the new propellant.



Figure 22. Hybrid rocket motor during functioning.

Following the test, it was observed that the entire grain burned completely, with no remaining unburned pieces or areas where the combustion was more intense or less intense. The variation in thrust was extracted from the data acquisition system, and it is displayed in the figure below.

Following the tests performed, the plot from Figure 23 presents the variation of the thrust and the pressure inside the rocket engine.

The results obtained following the tests show that the rocket engine worked without destroying itself, and the parameters obtained correspond to those resulting from the theoretical models from the literature.

From Figure 23, there are six visible time periods with different pressure thrust levels:

1: Oxygen flow is off, and igniter is off;

2: Oxygen flow is on, the igniter is off, and the motor acts as a cold jet thruster with low pressure and low thrust;

3: The igniter is fired and combustion starts. The pressure and thrust increase significantly. Thrust is almost constant. The burn is very clean, and the flame is invisible in the video, probably because of the high O/F ratio;

4: Thrusts decrease gradually. Some spikes are identified in the recording, probably indicating that some fuel may have detached from the internal surface of the combustion chamber;

5: The fuel is fully consumed. Thrust and pressure are caused only by oxygen flow. Levels are significantly higher than in the “2” interval because the hot combustion chamber is increasing the temperature of the oxygen;

6: The Solenoid valve cuts the oxygen flow. The test is complete.

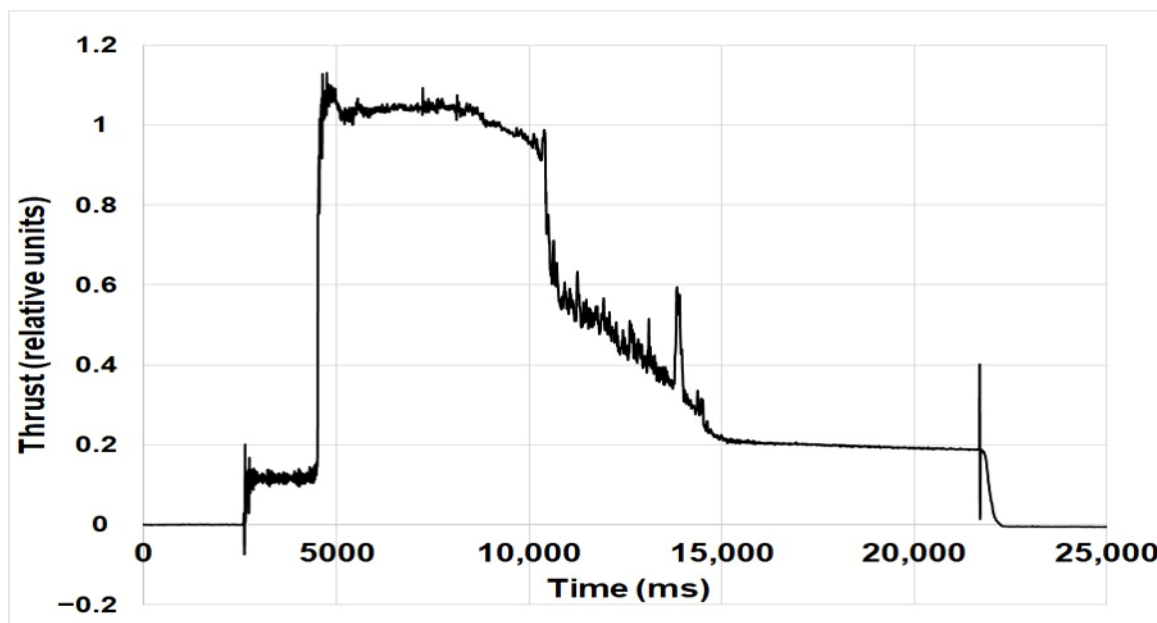


Figure 23. Thrust plots over rocket engine functioning time.

4. Discussion

One of the main concerns with paraffin-based fuels is their poor mechanical characteristics. Thus, the addition of additives to enhance the mechanical performance of paraffin for use in hybrid rocket engines represents an open field [3,35]. The limitations of paraffin-based fuel for hybrid rockets necessitate an exploration of additives to improve regression rates without compromising mechanical properties [30,35]. This study investigates the mechanical and microstructural aspects of the novel paraffin-based propellant in comparison with pure paraffin, both before and after exposure to negative temperatures. Understanding these characteristics is essential for optimizing the material's performance and ensuring its reliability in the demanding conditions of hybrid rocket propulsion systems.

Tensile testing results revealed significant variations in load, ultimate tensile strength, tensile elongation, and Young Modulus among different specimens. Samples M_c exhibited the highest load and UTS, indicating superior strength compared to the pure paraffin specimens. This heightened strength can be attributed to a combination of factors such as material composition, reinforcing agents, and specific processing conditions during fabrication. Therefore, adding additives is not always beneficial in all respects; Y. Pal et al. [35] found that adding Al and B did not significantly improve the regression rate of the propellant. In contrast, in another study [28], they demonstrated that these additives could enhance the compressive modulus and strength of the paraffin-based fuel formulations. Several studies have explored different additives to enhance the mechanical performance of paraffin-based fuels, but the influence varied as a function of material and concentration. One additive that has shown promising results is ethylene vinyl acetate (EVA). Kumar and Ramakrishna [36] achieved a 50% increase in tensile strength by adding 20% EVA to pure wax, while Maruyama et al. [37] reported a 1.6-times increase. Tang et al. [30] investigated the influence of adding six different types of additives, including stearic acid, polyethylene

wax (A-C6A), ethylene vinyl acetate copolymer (EVA), low-density polyethylene (LDPE), polypropylene (PP), and high-density polyethylene (HDPE) to paraffin fuel. They observed that the mechanical properties were enhanced based on the type of additive and increasing additive mass percentage. The optimal choice for improving compressive strength by 64% relative to pure paraffin was found to be adding a 5% mass of A-C6A to the paraffin matrix, while LDPE proved to be the most effective in enhancing tensile strength, showing an increase of 105.7% with the same mass addition. In other studies, it has been observed that the use of additives (e.g., carbon) contributed to a decrease in mechanical properties [35] due to the weak interfacial adhesion between the CB filler and paraffin matrix.

However, in this study, the addition of 10% stearic acid and 2% coal powder to the paraffin matrix resulted in increased tensile, compression, and flexural strength at both room and sub-zero temperatures. Tensile strength increased by 28% at room temperature and an impressive 102% at sub-zero temperature compared to pure paraffin. Similarly, the compression strength at room temperature and sub-zero temperature of the new propellant increased by 119% and 55%, respectively, compared to pure paraffin. Additionally, the flexural strength at room temperature and sub-zero temperature of the new propellant increased by 42% and 24%, respectively. These findings highlight the robust performance of the new propellant under both ambient and negative temperatures. The higher UTS of M_c suggests enhanced molecular cohesion and resistance to deformation, making it capable of withstanding higher tensile loads before failure. The influence of temperature on mechanical behavior aligns with findings in other studies [25,35], prompting further exploration of temperature effects on various properties and microscopic characteristics. Compression and three-point bend testing also showed variations in strength and elongation among specimens. The notably higher strength of the new propellant (M_c specimens), especially in cold conditions, aligns with expectations and underscores the potential advantages of the new propellant. Macrostructural examination showed a predominantly homogeneous structure with localized impurities and micro-voids. In other cases where additives were used in paraffin mixtures, it was observed that paraffin lumps can form, and the connections between these lumps are not dense, acting as mechanical failure concentrators [35]. However, the increased mechanical properties are caused by the strong interfacial interaction between the stearic acid, the coal, and the paraffin matrix.

Despite these features, their negligible impact on mechanical strength underscores the material's resilience. In contrast, Piscitelli et al. [26] developed four different paraffin waxes in a separate study and reported that the central region of their paraffin samples exhibited traces of pellets, partial liquefaction, and large and numerous internal micro-voids and micro-cracks. They suggested the necessity for both external mechanical pressure and thermal loads, reaching a bulk temperature of at least 110 °C, to address manufacturing challenges. Although the investigations in this study did not identify a significant issue with micro-voids, these measures could be considered in future studies to improve the quality of the newly developed propellant. Also, the data on the structural performance of the new propellant are insufficient to accurately predict the loads experienced during flight. Considering the varying stress strains, axial thrust loads, and radial combustion pressures that will be encountered during full-scale engine operation [35], a comprehensive examination of mechanical performance under these conditions, as well as a thermal characterization, is needed in the near future.

Scanning electron microscopy (SEM) analysis highlights the microstructural features, showcasing similarities between pure paraffin and the new propellant. The increased densification and reduced voids after cold treatment aligns with expectations, reinforcing the material's adaptability to varying mechanical loads. However, the addition of the stearic acid and coal to the paraffin matrix improves the mechanical interfacial resistance. This observation resonates with findings in [3,35,38] suggesting a common trend in propellant materials with added additives.

The investigation of fracture surfaces on specimens tested at room temperature revealed a generally more brittle appearance compared to those tested at sub-zero temper-

atures. The variation of ductility as a function of exposure and test temperature is also supported by the results of the tensile and compression mechanical testing, in which specimens tested at cold temperatures had significantly higher deformation than those tested at room temperature.

These results open new future research directions, including exploring manufacturing conditions, incorporating additional additives, and examining the effects of nozzle temperatures on mechanical properties. Additional microscopy investigations can evaluate impurity origins and distributions, advancing the understanding of the material's structural characteristics.

Regarding the performance of the new propellant, as observed from the numerical simulations, there is very little difference compared to the performance of pure paraffin. Similar to the approach in [35], where the enhancement of properties was achieved by adding coal and MgB₂ to paraffin, in this study, the improvement of mechanical performance was realized through an innovative new formula by adding stearic acid and coal without compromising the rocket engine's performance. This type of propellant is considered environmentally friendly, aligning with the pursuit of obtaining solid or hybrid propellants with high specific impulse that are non-polluting [11].

Regarding the combustion products of the new propellant, it was observed through simulations that there were no traces of ammonia, hydrochloric acid, or aluminum, making it an environmentally friendly propellant, unlike other solid propellants presented in [12]. For the simulated engine varying the O/F ratio, the resulting components included H₂, H₂O, O₂, CO₂, CO, and other combinations in insignificant proportions, unlike other propellants presented in [7–10].

Regarding the testing of the new propellant in the rocket engine on the test bench, this test proceeded under normal conditions, presenting a thrust-versus-time graph similar to other experienced propellants.

Future testing will be attempted with liquid oxygen to achieve comparable or enhanced performance of the engine.

5. Conclusions

Following the analysis of the new propellant through numerical simulations, it was observed that the addition of stearic acid and coal powder does not significantly degrade the performance compared to pure paraffin. The peak specific impulse is attained for both propellants at an O/F ratio of approximately 2.2. This ratio was also utilized in the experimental phase. Additionally, it was found that, during the combustion reaction as a function of O/F, there are no toxic substances such as ammonia, chlorine-based substances, or aluminum, as seen in the case of other solid propellants. The resulting components for the simulated motor include H₂, H₂O, O₂, CO₂, CO, and other combinations in insignificant percentages. It is worth noting that the CO concentration decreases with an increase in the O/F ratio for both propellants, and the differences between concentrations are not significant. Additionally, the CO₂ concentration peaks at an O/F ratio of around 4.7. The experimental test on the laboratory test bench did not record any unpleasant events, ensuring the integrity of both the motor and the test stand was not compromised.

The consistent trends observed under varying testing conditions establish a foundation for practical application, especially in low-temperature environments. This discussion sets the stage for future investigations and highlights the potential impact of the developed propellant on advancing hybrid rocket engine technology.

Tensile, compression, and three-point bend testing consistently highlight superior strength under ambient and cold-temperature conditions, highlighting the propellant's suitability for hybrid rocket engine applications.

The analysis of the mechanical tests provides valuable insights into material strength and ductility. Macrostructural, coupled with microstructural, examinations by SEM provide a clear view of the material's internal structure, highlighting its resilience despite minimal imperfections and a strong interfacial interaction between the stearic acid, coal, and paraffin

matrix. These findings position the developed propellant as a promising candidate for cold-temperature applications in hybrid rocket technology, and also pave the way for future advancements.

Author Contributions: Conceptualization, G.C. and A.P.; software, A.M.; validation, G.C., A.P., A.N.B. and A.I.H.; data curation, A.P., G.C., A.N.B., A.I.H. and T.F.F.; writing—original draft preparation, G.C., A.P., A.N.B. and A.I.H.; writing—review and editing, G.C., A.P., A.N.B. and A.I.H. All authors have read and agreed to the published version of the manuscript.

Funding: This research was performed within the “Nucleu” Programme, part of the National Plan for Research, Development and Innovation 2022–2027, carried out with the support of the Romanian Ministry of Research, Innovation and Digitalisation, project no. PN 23.12.06.02.

Data Availability Statement: Data are contained within the article.

Conflicts of Interest: The authors declare no conflicts of interest. Adrian Nicolae Buturache is the Founder & Research Data Scientist of FasterEdu. The company had no role in the design, collection, analyses, or interpretation of data, the writing of the manuscript, or the decision to publish the results.

References

1. Srivastava, S.; Thakur, A.K. Review on Hybrid Rocket Engine: Past, Present and Future Scenario. *Int. J. Veh. Struct. Syst.* **2022**, *14*, 680–685. [CrossRef]
2. Okninski, A. On use of hybrid rocket propulsion for suborbital vehicles. *Acta Astronaut.* **2018**, *145*, 1–10. [CrossRef]
3. Pal, Y.; Mahottamananda, S.N.; Palateerdham, S.K.; Subha, S.; Ingenito, A. Review on the regression rate-improvement techniques and mechanical performance of hybrid rocket fuels. *FirePhysChem* **2021**, *1*, 272–282. [CrossRef]
4. Barato, F. Review of Alternative Sustainable Fuels for Hybrid Rocket Propulsion. *Aerospace* **2023**, *10*, 643. [CrossRef]
5. Chandler, A.A.; Cantwell, B.J.; Hubbard, G.S.; Karabeyoglu, A. Feasibility of a single port Hybrid Propulsion system for a Mars Ascent Vehicle. *Acta Astronaut.* **2011**, *69*, 1066–1072. [CrossRef]
6. Rugescu, R.; Coman, C.; Bogoi, A.; Farcasan, I.; Constantinescu, D. Hybrid Rocket Engine Novel Technology for the Orbital Launcher NERVA. In Proceedings of the 3rd International Conference on Experiments/Process/System Modeling/Simulation, Athens, Greece, 8–11 July 2009.
7. Kositsyna, O.S.; Dron', M.M.; Yemets, V. The environmental impact assessment of emission from space launches: The promising propellants components selection. *J. Chem. Technol.* **2020**, *28*, 186–193. [CrossRef]
8. Terry, B.C.; Sippel, T.R.; Pfeil, M.A.; Gunduz, I.E.; Son, S.F. Removing hydrochloric acid exhaust products from high performance solid rocket propellant using aluminum-lithium alloy. *J. Hazard. Mater.* **2016**, *317*, 259–266. [CrossRef]
9. Vellaisamy, U.; Shelly, B. Effect of metal additives on neutralization and characteristics of AP/HTPB solid propellants. *Combust. Flame* **2020**, *221*, 326–337. [CrossRef]
10. Gohardani, A.S.; Stanojev, J.; Demairé, A.; Anflo, K.; Persson, M.; Wingborg, N.; Nilsson, C. Green space propulsion: Opportunities and prospects. *Prog. Aerosp. Sci.* **2014**, *71*, 128–149. [CrossRef]
11. Cican, G.; Mitrache, A.-D. Rocket Solid Propellant Alternative Based on Ammonium Dinitramide. *INCAS Bull.* **2017**, *9*, 17–24.
12. Wingborg, N.; de Flon, J.; Johnson, C.; Whitlow, W. Green Propellants Based on AND. In Proceedings of the Space Propulsion, Heraklion, Greece, 5–8 May 2008.
13. Thomas, J.C.; Paravan, C.; Stahl, J.M.; Tykol, A.J.; Rodriguez, F.A.; Galfetti, L.; Petersen, E.L. Experimental evaluation of HTPB/paraffin fuel blends for hybrid rocket applications. *Combust. Flame.* **2021**, *229*, 111386. [CrossRef]
14. Jens, E.T.; Cantwell, B.J.; Hubbard, G.S. Hybrid rocket propulsion systems for outer planet exploration missions. *Acta Astronaut.* **2016**, *128*, 119–130. [CrossRef]
15. Veale, K.; Adali, S.; Pitot, J.; Brooks, M. A review of the performance and structural considerations of paraffin wax hybrid rocket fuels with additives. *Acta Astronaut.* **2017**, *141*, 196–208. [CrossRef]
16. Evans, B.; Boyer, E.; Kuo, K.; Risha, G.; Chiaverini, M. Hybrid rocket investigations at Penn state University's high pressure combustion laboratory: Overview and recent results. In Proceedings of the 45th AIAA/ASME/SAE/ASEE Joint Propulsion Conference & Exhibit, Denver, CO, USA, 2–5 August 2009; pp. 1–22.
17. Galfetti, L.; Merotto, L.; Boiocchi, M.; Maggi, F.; Deluca, L.T. Experimental investigation of paraffin-based fuels for hybrid rocket propulsion. *Prog. Propuls. Phys.* **2013**, *4*, 59–74.
18. Schultz, R.G. Hybrid Rocket Motor (HRM) Test Stand: An Investigation of the Effects of Additives, Department of Aerospace Engineering, The University of Arizona August 2013. Available online: https://repository.arizona.edu/bitstream/handle/10150/311821/azu_etd_mr_2013_0296_sip1_m.pdf?sequence=1&isAllowed=y (accessed on 12 December 2023).
19. Kim, S.; Lee, J.; Moon, H.; Sung, H.; Kim, J. Effect of paraffin-LDPE blended fuel in hybrid rocket motor. In Proceedings of the 46th AIAA/ASME/SAE/ASEE Joint Propulsion Conference & Exhibit, Nashville, TN, USA, 25–28 July 2010; pp. 1–16.
20. Mazzetti, A.; Merotto, L.; Pinarello, G. Paraffin-based hybrid rocket engines applications: A review and a market perspective. *Acta Astronaut.* **2016**, *126*, 286–297. [CrossRef]

21. Cardoso, K.P.; Ferrão, L.F.A.; Kawachi, E.Y.; Araújo, T.B.; Nunes, R.F.; Nagamachi, M.Y. Preparation of paraffin-based solid combustible for hybrid propulsion rocket motor. *J. Propuls. Power* **2016**, *33*, 448–455. [[CrossRef](#)]
22. Kobald, M.; Schmierer, C.; Ciezki, H.K.; Schlechtriem, S.; Toson, E.; De Luca, L.T. Viscosity and regression rate of liquefying hybrid rocket fuels. *J. Propuls. Power* **2017**, *33*, 1245–1251. [[CrossRef](#)]
23. Kobald, M.; Verri, I.; Schlechtriem, S. Theoretical and experimental analysis of liquid layer instability in hybrid rocket engines. *CEAS Space J.* **2015**, *7*, 11–22. [[CrossRef](#)]
24. Kim, S.; Moon, H.; Kim, J.; Cho, J. Evaluation of paraffin–polyethylene blends as novel solid fuel for hybrid rockets. *J. Propuls. Power* **2015**, *31*, 1750–1760. [[CrossRef](#)]
25. Veale, K.; Adali, S.; Pitot, J.; Bemont, C. The structural properties of paraffin wax based hybrid rocket fuels with aluminium particles. *Acta Astronaut.* **2018**, *151*, 864–873. [[CrossRef](#)]
26. Piscitelli, F.; Saccone, G.; Gianvito, A.; Cosentino, G.; Mazzola, L. Characterization and manufacturing of a paraffin wax as fuel for hybrid rockets. *Propuls. Power Res.* **2018**, *7*, 218–230. [[CrossRef](#)]
27. Andrianov, A.; Lee, J.; Shynkarenko, O.; Simone, D.; De Moraes Bertoldi, A.E. Experimental study of severity level of structural discontinuities in paraffin grains of hybrid propellant rocket. *Acta Astronaut.* **2019**, *162*, 256–265. [[CrossRef](#)]
28. Pal, Y.; Kumar, K.H.; Li, Y.H. Ballistic and mechanical characteristics of parafn based solid fuels. *CEAS Space J.* **2019**, *11*, 317–327. [[CrossRef](#)]
29. Tang, Y.; Chen, S.; Zhang, W.; Shen, R.; DeLuca, L.T.; Ye, Y. The Effects of Mechanical Modification Additives on the Regression Rate of Paraffin-Based Fuels for Hybrid Rocket. In Proceedings of the 7th European Conference for Aeronautics and Space Sciences (EUCASS), Milan, Italia, 3–6 July 2017.
30. Tang, Y.; Chen, S.; Zhang, W.; Shen, R.; DeLuca, L.T.; Ye, Y. Mechanical Modifications of Paraffin-based Fuels and the Effects on Combustion Performance. *Propellants Explos. Pyrotech.* **2017**, *42*, 1268–1277. [[CrossRef](#)]
31. Borowski, G. Possibilities of Utilization of Energy Briquettes. *Electr. Eng. Res. Report.* **2011**, *1*, 48–51.
32. Sutton, G.P.; Biblarz, O. *Rocket Propulsion Elements*, 7th ed.; Published John Wiley & Sons, Inc.: New York, NY, USA, 2013; p. 494.
33. Cican, G.; Popa, I.F.; Buturache, A.N.; Hapenciuc, A.I. Design, Manufacturing, and Testing Process of a Lab Scale Test Bench Hybrid Rocket Engine. *Eng. Technol. Appl. Sci. Res.* **2023**, *13*, 12039–12046. [[CrossRef](#)]
34. Bogoi, A.; Rugescu, R. Modelling transients in rocket engines by enhanced high-order. In Proceedings of the 1st International Conference on Manufacturing Engineering, Quality and Production Systems (Volume II), Brasov, Romania, 24–26 September 2009.
35. Pal, Y.; Palateerdhamb, S.K.; Mahottamanandac, S.N.; Sivakumara, S.; Ingenitob, A. Combustion performance of hybrid rocket fuels loaded with MgB2 and carbon black additives. *Propuls. Power Res.* **2023**, *12*, 212–226. [[CrossRef](#)]
36. Kumar, R.; Ramakrishna, P.A. Studies on EVA-based wax fuel for launch vehicle applications. *Propellants Explos. Pyrotech.* **2016**, *1*, 295–303. [[CrossRef](#)]
37. Maruyama, S.; Ishiguro, T.; Shinohara, K.; Nakagawa, I. Study on Mechanical Characteristics of Paraffin-Based Fuel. In Proceedings of the 47th AIAA/ASME/SAE/ASEE Joint Propulsion Conference & Exhibit, San Diego, CA, USA, 31 July–3 August 2011; American Institute of Aeronautics and Astronautics: Reston, VA, USA, 2011. AIAA-2011-5678.
38. Ryu, S.; Han, S.; Kim, J.; Moon, H.; Kim, J.; Ko, S.W. Tensile and compressive strength characteristics of aluminized paraffin wax fuel for various particle size and contents. *Korean Soc. Propuls. Eng.* **2016**, *20*, 70–76. [[CrossRef](#)]

Disclaimer/Publisher’s Note: The statements, opinions and data contained in all publications are solely those of the individual author(s) and contributor(s) and not of MDPI and/or the editor(s). MDPI and/or the editor(s) disclaim responsibility for any injury to people or property resulting from any ideas, methods, instructions or products referred to in the content.